Retrieval of Three-Dimensional Particle Velocity from Airborne Doppler Radar Data

D. LEON AND G. VALI

Department of Atmospheric Science, University of Wyoming, Laramie, Wyoming

(Manuscript received 28 April 1997, in final form 28 September 1997)

ABSTRACT

A technique has been developed for the retrieval of three-dimensional particle velocities from Doppler data obtained with an airborne radar. The 95-GHz radar was mounted on the University of Wyoming KingAir aircraft. The retrieval technique is derived from the velocity azimuth display (VAD) analysis and is termed the airborne velocity azimuth display (AVAD). Data for this analysis are taken when the radar beam is scanned by the turning of the aircraft. As in VAD analysis, a functional form for the horizontal variation of the velocity of the scatterers must be assumed. The components of the velocity field are then determined using a least squares fit to the Doppler velocities. The AVAD technique differs from VAD analysis because of the mobility of the platform and its proximity to regions of interest, and it is due to geometric considerations dictated by the turning of the aircraft. The analysis region is only a few kilometers in diameter—considerably smaller than for a ground-based VAD analysis. This reduces the required area of cloud coverage and the importance of horizontal variations in the wind field. However, the reduced analysis area also limits the accuracy with which higher-order characteristics of the wind field, such as divergence, can be resolved.

This paper presents the AVAD technique and describes the data processing required. Results from multiple AVAD analyses from flights on two days are presented and are shown to be in generally good agreement with winds measured by sensors on board the KingAir.

1. Introduction

Knowledge of air motions is fundamental for the understanding of the microphysical and dynamic processes that determine the evolution of clouds and storm systems. Consequently, a wide variety of techniques has been developed to measure the winds. Different techniques give either profiles of winds as a function of height or two- or three-dimensional wind fields.

Radiosondes and aircraft-based soundings are some of the most common means of obtaining wind profiles. These soundings also provide valuable thermodynamic information; however, the measurements are taken along a line, making it difficult to assess the variability of the measurements and how representative they are of the volume.

Where there are sufficient scatterers, wind profiles and wind fields can also be determined through the use of Doppler radars and their derivatives. The fundamental limitation of Doppler radars, that they only measure the radial component of velocity, can be overcome with the use of two common approaches. The first involves the use of multiple Doppler radars (or one mobile radar) that observe the same volume from multiple angles. The second approach makes use of a single Doppler radar combined with assumptions about the horizontal form of the wind field.

Multiple-Doppler techniques allow three-dimensional winds to be calculated over a grid. This allows the spatial variability of the wind field on scales greater than the grid spacing to be observed directly, while variations smaller than the grid spacing are averaged. Ground-based dual-Doppler radar analysis is restricted to a small region determined by the location of the radars. Airborne multiple-Doppler analyses, such as described by Jorgensen et al. (1996), take place over much larger regions. The analysis region is determined by the aircraft flight pattern, rather than being dictated by a fixed radar location.

The velocity azimuth display (VAD) technique analysis is an example of the second type of approach to resolving winds from Doppler radar. This is one of the earliest applications of Doppler radar. The VAD technique was described by Probert-Jones (1960) and Lhermitte and Atlas (1961) and later discussed in more detail by Browning and Wexler (1968). A single radar is scanned in azimuth while mantaining a fixed elevation angle, thus the data come from a thin shell of a cone emanating from the radar. The wind profiles retrieved can be argued (through the use of the divergence theorem) to be representative of the volume. Wind profilers can be considered to be a degenerate adaptation of the VAD analysis, where the velocity is sampled in only three or four different azimuths. Generally, low elevation angles are used in the VAD analysis to limit the contribution of particle fallspeeds to the Doppler velocities. The low elevation angles combined with the distance from the radar to the regions of interest result in a large area over which the VAD analysis is done.

Corresponding author address: Mr. David Leon, Department of Atmospheric Science, University of Wyoming, Box 3038, Laramie, WY 82071.

TABLE 1. University of Wyoming millimeter radar specifications.

Characteristic	Value	Units	Comments
Wavelength	3.16	mm	
Transmit frequency	94.92	GHz	
Antenna diameter	0.305	m	
Antenna beamwidth	0.7°		
Antenna gain	49	dB	
Sidelobes	−31	dB	
Radar beam orientation			
Up-looking	2.8°		Forward of vertical
Side-looking	−1.0°		Forward of right
Peak transmit power	1.2	kW	
Pulse duration	250	ns	
Pulse repetition frequency	20 000	Hz	Maximum
Receiver bandwidth	5	MHz	
Minimum detectable signal	−25	dBZ	At 1 km
Samples averaged	400		Typical
Unambiguous range	7.5	km	Minimum
Unambiguous velocity	31.8	m s^{-1}	Maximum
Range resolution	37.5	m	250-ns pulse
Alongtrack resolution	5	m	Typical

The millimeter radar mounted on the University of Wyoming KingAir aircraft allows for the development of a VAD-based technique. The radar antenna is mounted so as to produce a beam that points to the right of the aircraft. The radar beam can be redirected upward by means of a reflector plate. This radar uses a short 3.16-mm wavelength that allows a narrow 0.7° beam with a reasonably small (0.3 m) antenna. However, this wavelength is much more strongly attenuated by liquid water than longer wavelengths. Details of the radar implementation are included in Table 1.

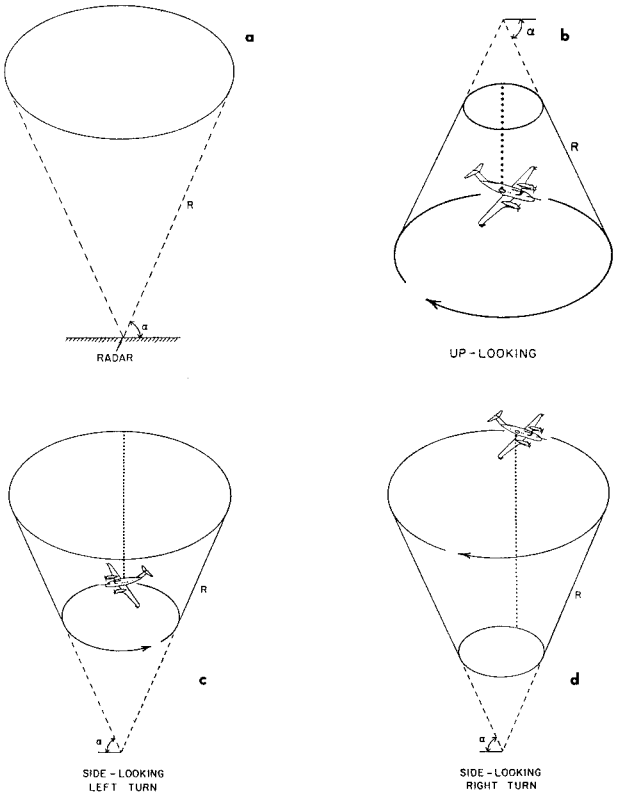

FIG. 1. Scanning geometry for (a) ground-based radar, (b) up-looking radar beam (left or right turn), (c) side-looking radar beam (left turn), and (d) side-looking radar beam (right turn).

The fixed orientation of the radar beam prevents the adaptation of airborne multiple-Doppler radar techniques to this case. However, the radar beam can be scanned by turning the aircraft. The aircraft bank during a turn results in a scanning geometry similar to that of a ground-based radar scanning in azimuth. The effective elevation angle of the scan is controlled by the roll angle of the aircraft, which in turn is determined by airspeed and turn radius. Thus, this angle cannot be selected for purely meteorological reasons. The geometry of the radar beam during a turn is shown in Fig. 1. Depending on the turn direction and the radar beam orientation, the radar beam describes a cone that converges above the flight track (up-looking beam, either turn direction), a cone that converges below the flight track (side-looking beam, right turn), or a cone that diverges above the flight track (side-looking beam, left turn).

The similarity between the ground-based and airborne geometries implies that VAD analysis can be adapted to the airborne case and leads the authors to call this the airborne velocity azimuth display (AVAD) technique. Radar data from a turn are broken into data subsets corresponding to a constant altitude, and the analysis is carried out separately for each level.

The diameter of the analysis region is determined primarily by the diameter of the turn, beam orientation, and turn direction. Typically, the diameter of the turn is roughly 3 km for a roll angle of 30°. This generally results in an analysis region with a diameter between 0.5 and 4 km, although the analysis region may become as large as 10 km for the side-looking left turn case. The typical range gate spacing of 30 m gives a vertical

resolution of about 20 m. Thus, the AVAD technique is a cloud-scale tool that can provide high vertical resolution wind profiles with less than 60 seconds' worth of data. These profiles provide a context for the data gathered by the in situ probes mounted on the aircraft and partially bridge the gap in scale between the data gathered by the in situ probes and data gathered by other tools, such as ground-based radars.

The data used in this paper come from two cases: a nimbostratus case studied in Wyoming in 1992 and a stratus case from off the Oregon coast that was studied in 1995. The in situ winds measured from the KingAir will be used for comparisons with the results of the AVAD analysis.

2. Data processing

a. Beamvector notation

The complexity involved in describing the orientation of the radar beam when the aircraft is not flying straight and level prompts the introduction of a simplifying notation, the development of the notation presented in this section parallels that of Lee et al. (1994). The beamvector, **b**, is a unit vector aligned along the center of the radar beam. The width of the radar beam, while finite, is sufficiently small so that for most purposes the beam can be treated as a line. The measured Doppler velocity can be written in terms of **b** as

$$V_{\text{Dopp}} = \mathbf{b}\cdot\mathbf{V}_{\text{p}}, \tag{1}$$

where $\mathbf{V}_{\text{p}}$ is the three-dimensional velocity of the scatterers relative to the platform. For a ground-based radar the components of **b** can be written in terms of the azimuth (ϕ) and elevation (α) angles as

$$\begin{aligned} b_x &= \cos(\alpha)\cos(\phi), \\ b_y &= \cos(\alpha)\sin(\phi), \quad \text{and} \\ b_z &= \sin(\alpha), \end{aligned} \tag{2}$$

where b_x, b_y, and b_z refer, respectively, to the east, north, and vertical components of **b**.

Given aircraft orientation and attitude data—pitch, roll, and heading angles—the beamvector in aircraft coordinates, $\mathbf{b}_{\text{ac}}$, can be transformed into ground coordinates, $\mathbf{b}_{\text{gr}}$. This coordinate transformation is accomplished through the use of three rotations about each of the aircraft axes (Lenschow 1971),

$$\mathbf{b}_{\text{gr}} = \mathbf{T}\mathbf{b}_{\text{ac}}, \tag{3}$$

where **T** is the transformation matrix, which in turn can be expressed as the product of three transformation matrices about the aircraft axes:

$$\mathbf{T} = \mathbf{H}\,(\mathbf{PR}), \tag{4}$$

with the matrices **H**, **P**, and **R** given by

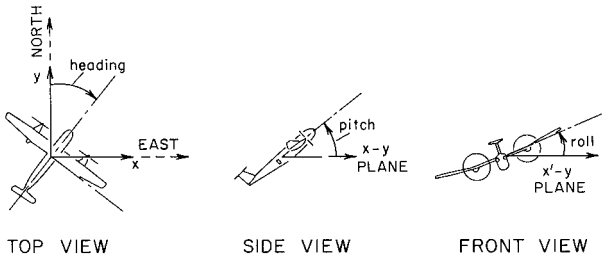

FIG. 2. Heading (ψ), pitch (θ), and roll (ϕ) angles [adapted from Lenschow (1971)].

$$\mathbf{R} = \begin{pmatrix} 1 & 0 & 0 \\ 0 & \cos(\phi) & -\sin(\phi) \\ 0 & \sin(\phi) & \cos(\phi) \end{pmatrix}, \tag{5}$$

$$\mathbf{P} = \begin{pmatrix} \cos(\theta) & 0 & \sin(\theta) \\ 0 & 1 & 0 \\ -\sin(\theta) & 0 & \cos(\theta) \end{pmatrix}, \quad \text{and} \tag{6}$$

$$\mathbf{H} = \begin{pmatrix} \sin(\psi) & \cos(\psi) & 0 \\ \cos(\psi) & -\sin(\psi) & 0 \\ 0 & 0 & -1 \end{pmatrix}, \tag{7}$$

where ψ, θ, and ϕ are the heading, pitch, and roll angles, respectively, as defined in Fig. 2. In this application $\mathbf{b}_{\text{ac}}$ is constant, thus only **T** must be computed to obtain the instantaneous value of $\mathbf{b}_{\text{gr}}$. Hereafter, **b** will be used to refer to the beamvector in ground coordinates, unless otherwise noted.

b. Correction for aircraft motion

Doppler velocity is measured with respect to the aircraft. Unless the aircraft velocity is perpendicular to **b**, the measured Doppler velocity is not the same as would be measured by a fixed radar. To express the velocity in a ground-relative frame, the component of the aircraft motion in the Doppler velocity must be removed. Using the notation introduced in the previous section, the Doppler velocity measured from the aircraft can be expressed as

$$\mathrm{V}_{\text{Dopp}} = \mathbf{b}\cdot\mathbf{V}_{\text{p}} - \mathbf{b}\cdot(\mathbf{V}_{\text{ac}} + \Omega_{\text{ac}} \times \mathbf{R}_{\text{radar}}), \tag{8}$$

where $\mathbf{V}_{\text{ac}}$ is the aircraft velocity vector, Ω_{ac} is the aircraft rotation rate vector, and $\mathbf{R}_{\text{radar}}$ is the moment arm from the inertial navigation system (INS) to the radar. The second term on the right-hand side of Eq. (8) represents the contribution of the aircraft motion to the Doppler velocity. The sum ($\mathbf{V}_{\text{ac}} + \Omega_{\text{ac}} \times \mathbf{R}_{\text{radar}}$) is the velocity at the radar.

The horizontal components of $\mathbf{V}_{\text{ac}}$ are determined from INS and GPS data. GPS data are used for the low-frequency components (those less than 0.02 Hz), and INS data are used for higher frequencies. The vertical component of the aircraft velocity is calculated from the INS vertical acceleration and pressure data. The aircraft attitude (pitch, roll, and heading) and the rotation rate (pitch rate, roll rate, and heading change rate) are derived from the INS.

The aircraft velocity $\mathbf{V}_{ac}$ is generally close to an order of magnitude greater than the velocity of the target, thus both $\mathbf{V}_{ac}$ and $\mathbf{b}$ must be accurately known, otherwise errors in the aircraft motion removal might result in errors that are significantly larger than the velocity of the targets.

A precise determination of the beamvectors in aircraft coordinates must be made. An error of only 1° along the flight track will cause a bias of 1.5 m s^{-1} in the Doppler velocity at a typical aircraft speed of 90 m s^{-1}. The antenna installation was designed to result in a beam oriented 3.6° forward of the vertical in the up-looking case or to the right (perpendicular to the aircraft centerline) in the side-looking case. The up-looking beam orientation was chosen to compensate for the typical angle of attack of the aircraft, thus resulting in a true vertically pointing beam during straight and level flight.

However, the installation could not be assumed to be sufficiently accurate, and direct measurements of the beam orientation were needed. The high velocity of the aircraft can be used to an advantage in determining the beam orientation by the Doppler velocity of a target of known velocity. The side-looking beam orientation is determined by using the ground as a velocity reference. Here, $\mathbf{b}_{ac_{side}}$ is set to minimize the residual velocity of the ground. Determination of the up-looking beam orientation is significantly more difficult than the side-looking case due to the absence of a convenient velocity reference. During the Small Cumulus Microphysics Study (SCMS) project the KingAir flew under the Merlin aircraft (operated by Météo-France) and received a radar return from it. This aircraft carries both INS and GPS navigation equipment and could therefore be used as a velocity reference. The $\mathbf{b}_{up}$ is set to satisfy the following relationship:

$$V_{Dopp} = \mathbf{b}_{up} \cdot (\mathbf{V}_{Merlin} - \mathbf{V}_{KingAir}). \quad (9)$$

The up-looking beam has been calculated to point 3.0° forward of up, while the side-looking beam has been estimated to point 1.0° back of right.

The determination of the beam orientations has focused on the alignment of the beams along the aircraft centerline. This is the most critical component of the beam orientation; however, there is potential for the beam to be misaligned perpendicular to the aircraft centerline. That is, the up-looking beam may be misaligned to the left or right of vertical, while the side-looking beam may be misaligned above or below the horizontal. This is not as significant for the side-looking beam case since the maximum vertical speeds of both the scatterers and the aircraft are not very large compared to their horizontal speeds. However, in the up-looking case a misalignment could be significant as horizontal velocities can be large, whereas vertical velocities are generally small. Unfortunately, it is extremely difficult to evaluate these errors.

The accuracy with which the pitch and roll angles are known is limited by the Schuler oscillation. A Schuler oscillation of (peak–peak) amplitude of 5 km corresponds approximately to a 0.02° error in aircraft attitude. Currently, the pitch and roll angles are not corrected for the effects of the Schuler oscillation; however, these effects are close to an order of magnitude smaller than the uncertainties in beam orientation, which are believed to be about 0.25° and 0.4° for the side- and up-looking beams, respectively.

The component of aircraft motion in the measured Doppler velocities $[\mathbf{b} \cdot (\mathbf{V}_{ac} + \Omega_{ac} \times \mathbf{R}_{radar})]$ is calculated for each profile and corrected for in a separate processing step. Errors in both the beamvectors and the aircraft velocity translate into errors in the measured Doppler velocity.

The residual velocity of the ground once the aircraft motion has been removed is used to provide a quantitative assessment of the accuracy of the aircraft motion removal for the side-looking beam. The residual Doppler velocities of the ground are generally less than 0.4 m s^{-1}; however, high-frequency (>1 Hz) components of aircraft motion are not corrected as accurately (possibly due to timing problems), so the aircraft motion removal is significantly worse in turbulent conditions.

c. Constant altitude data subsets

The aircraft flies at varying altitudes and with varying roll and pitch angles, thus, a single range gate does not correspond to a fixed altitude. The position of the center of a radar gate, $\mathbf{X}_{gate}$, can be calculated from $\mathbf{b}$ and the aircraft position $\mathbf{X}_{ac}$:

$$\mathbf{X}_{gate} = r_{gate}\mathbf{b} + \mathbf{X}_{ac} \quad \text{and} \quad (10)$$

$$Z_{gate} = r_{gate} b_z + Z_{ac}. \quad (11)$$

This equation can be solved for the range to a given altitude:

$$r = \frac{Z - Z_{ac}}{b_z}. \quad (12)$$

A data subset is then constructed for an altitude by linearly interpolating between the range gates nearest the chosen altitude. Data subsets that are separated by more than twice the range gate spacing are completely independent.

3. The AVAD technique

a. Least squares solution

Once the Doppler velocity has been corrected for aircraft motion and data subsets corresponding to fixed altitudes have been constructed, then the inversion to determine the winds can be done. The traditional method for determining the wind field made use of Fourier analysis. The use of Fourier-type methods is not an option for the airborne analysis, as changing aircraft altitude and roll lead to irregular spacing of data points. Rather, a generalized least squares solution similar to the methods used by Easterbrook (1975) and Testud et al. (1980) is utilized. The least squares solution is significantly more robust than the spectral methods and can tolerate gaps in the data as well as irregular spacing. The least

squares solution requires that we be able to state the problem in the following form:

$$V_{Dopp} = \mathbf{G}\mathbf{V}, \tag{13}$$

where V_{Dopp} is a vector of the measured Doppler velocities, $\mathbf{G}$ is the forward matrix describing how the model parameters are weighted, and $\mathbf{V}$ is the vector to be retrieved.

The first step is to assume a functional form for $\mathbf{V}(x, y, t)$. The analysis is done separately for each altitude, so no assumption about the vertical variation of the velocity field is needed. Results from a series of altitudes are assembled into a profile.

The simplest form for the AVAD analysis is the horizontally homogeneous windfield:

$$\begin{aligned} V_x(x, y, t) &= V_{x_0}, \\ V_y(x, y, t) &= V_{y_0}, \quad \text{and} \\ V_z(x, y, t) &= V_{z_0}, \end{aligned} \tag{14}$$

where the terms V_{x_0}, V_{y_0}, and V_{z_0} are constant. Browning and Wexler (1968) presented a more sophisticated velocity field where the components of the velocity field vary linearly in the horizontal:

$$\begin{aligned} V_x(x, y, t) &= V_{x_0} + \overline{\frac{\partial V_x}{\partial x}}x + \overline{\frac{\partial V_x}{\partial y}}y, \\ V_y(x, y, t) &= V_{y_0} + \overline{\frac{\partial V_y}{\partial y}}y + \overline{\frac{\partial V_y}{\partial x}}x, \quad \text{and} \\ V_z(x, y, t) &= V_{z_0} + \overline{\frac{\partial V_z}{\partial x}}x + \overline{\frac{\partial V_z}{\partial y}}y. \end{aligned} \tag{15}$$

This form of the wind field allows for the determination of divergence as well as stretching and shearing deformations. The terms corresponding to horizontal variations of the vertical component have been added to the formulation of Browning and Wexler (1968) because with the higher elevation angles employed during this analysis, these components may become significant.

The equation for Doppler velocity at one altitude [Eq. (1)] can be rewritten in matrix form as

$$V_{Dopp} = \begin{bmatrix} b_x & b_y & b_z \end{bmatrix} \begin{bmatrix} V_x \\ V_y \\ V_z \end{bmatrix}. \tag{16}$$

A series of n measurements of the Doppler velocity with an assumed horizontally homogeneous windfield can be written as

$$\begin{bmatrix} V_{Dopp_1} \\ V_{Dopp_2} \\ V_{Dopp_3} \\ \vdots \\ V_{Dopp_n} \end{bmatrix} = \begin{bmatrix} b_{x_1} & b_{y_1} & b_{z_1} \\ b_{x_2} & b_{y_2} & b_{z_2} \\ b_{x_3} & b_{y_3} & b_{z_3} \\ \vdots & \vdots & \vdots \\ b_{x_n} & b_{y_n} & b_{z_n} \end{bmatrix} \begin{bmatrix} V_x \\ V_y \\ V_z \end{bmatrix}. \tag{17}$$

Similarly, for the linearly varying velocity field case, a series of measurements of the Doppler velocity can be written as

$$\begin{bmatrix} V_{Dopp_1} \\ V_{Dopp_2} \\ V_{Dopp_3} \\ \vdots \\ V_{Dopp_n} \end{bmatrix} = \begin{bmatrix} b_{x_1} & b_{y_1} & b_{z_1} & b_{x_1}x_1 & b_{y_1}y_1 & b_{x_1}y_1 & b_{y_1}x_1 & b_{z_1}x_1 & b_{z_1}y_1 \\ b_{x_2} & b_{y_2} & b_{z_2} & b_{x_2}x_2 & b_{y_2}y_2 & b_{x_2}y_2 & b_{y_2}x_2 & b_{z_2}x_2 & b_{z_2}y_2 \\ b_{x_3} & b_{y_3} & b_{z_3} & b_{x_3}x_3 & b_{y_3}y_3 & b_{x_3}y_3 & b_{y_1}x_3 & b_{z_3}x_3 & b_{z_3}y_3 \\ \vdots & \vdots & \vdots & \vdots & \vdots & \vdots & \vdots & \vdots & \vdots \\ b_{x_n} & b_{y_n} & b_{z_n} & b_{x_n}x_n & b_{y_n}y_n & b_{x_n}y_n & b_{y_n}x_n & b_{z_n}x_n & b_{z_n}y_n \end{bmatrix} \begin{bmatrix} V_x \\ V_y \\ V_z \\ \overline{\frac{\partial V_x}{\partial x}} \\ \overline{\frac{\partial V_y}{\partial y}} \\ \overline{\frac{\partial V_x}{\partial y}} \\ \overline{\frac{\partial V_y}{\partial x}} \\ \overline{\frac{\partial V_z}{\partial x}} \\ \overline{\frac{\partial V_z}{\partial y}} \end{bmatrix}. \tag{18}$$

Subsets of the terms in Eq. (18) can also be appropriately used for a given situation.

The matrix of beamvectors (for the selected form of the velocity field) is then inverted using a singular value decomposition (Bevington 1969; Menke 1989), such that

$$\mathbf{V}_{\text{est}} = \mathbf{G}^{-g}\mathbf{V}_{\text{Dopp}}. \tag{19}$$

The estimated velocity field parameters can then be used, together with the matrix of beamvectors, to produce an array of predicted Doppler velocities:

$$\mathbf{V}_{\text{Dopp}_{\text{pre}}} = \mathbf{G}\mathbf{V}_{\text{est}}. \tag{20}$$

Comparison between the predicted and actual data values can reveal how well the wind fields have been fit and the appropriateness of the velocity field form.

In our application the diameter of the analysis regions is reduced by an order of magnitude compared to a typical ground-based VAD analysis. This reduces the variation in the winds across the analysis domain caused by higher-order characteristics of the wind field. This makes the assumptions that must be made about the functional form of the wind field significantly less stringent but also reduces the accuracy with which the higher-order characteristics of the wind field can be determined. Thus, the horizontally homogeneous form for the wind field will be used in this paper. The vertical component of velocity, V_z, retrieved in this analysis is the vertical particle speed, which is the difference between the vertical wind component w and the terminal velocity of the scatterers V_t. No attempt to separate w from V_t is made due to the weaknesses inherent in attempting to utilize a Z–V_t relationship at W band and due to the high effective elevation angles used—increasing the importance of having an accurate Z–V_t relationship relative to low elevation angle applications.

b. Error analysis

The estimated value of the component of the velocity field is a sum of the input data weighted by the appropriate components of the inverse matrix. The ith parameter of the velocity field can be expressed as

$$\mathrm{V}_i = \sum_{j=1}^{n} G_{ij}^{-g}\mathrm{V}_{\text{Dopp}_j}. \tag{21}$$

The variance of the Doppler velocity can be used to calculate the variance of the estimated parameter. Turbulence with scales greater than the pulse volume leads to correlation between neighboring points. Thus, it would be inappropriate to assume that the data points were independent, rather it is assumed that the covariance between two data points is a function only of the time between the samples. Thus, the variance of the measured Doppler velocities can be estimated from the difference between the observed values, and the least squares fit can be predicted by the forward model and the estimated winds:

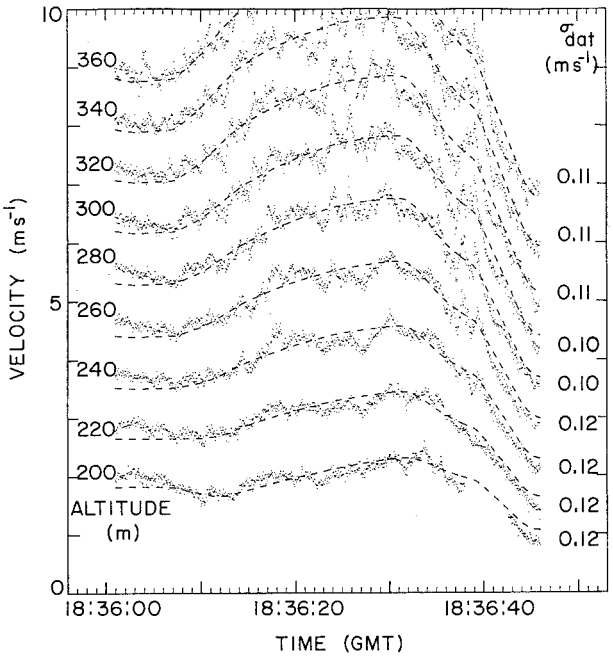

FIG. 3. Least squares fit (dashed line) and measured Doppler velocity (dots).

$$\sigma_d^2 = \frac{1}{n-m}\sum_{i=1}^{n}\left(\mathrm{V}_{\text{Dopp}_i} - \mathrm{V}_{\text{Dopp}_{\text{pre}_i}}\right)^2, \tag{22}$$

where m is the number of model parameters (three in the case of assumed horizontal homogeneity, nine for the linearly varying wind field). The value of σ_d generally falls in the range of 0.2–1 m s^{-1} for the stratiform cases presented; it seems probable that convective cases might have significantly greater σ_d. Figure 3 shows an example of the measured Doppler velocities and the least squares fit values for a range of altitudes. It is apparent in this figure that deviation of the winds about the least squares fit is not random, but rather consists of semiregular oscillations about the fit value.

The standard deviation of the wind field parameters can then be estimated given σ_d and the weights of the inverse matrix $\mathbf{G}^{-g}$:

$$\text{var}(\mathbf{V}_i) = \sum_{j=1}^{n}\sum_{k=1}^{n}\mathbf{G}_{ij}^{-g}\mathbf{G}_{ik}^{-g}\,\text{cov}(\mathrm{V}_{\text{Dopp}_j}, \mathrm{V}_{\text{Dopp}_k}). \tag{23}$$

Neighboring points are usually correlated because of turbulence, waves, and other velocity variations that are smaller than the area of the analysis but larger than the volume of a single pulse. The correlation between measurements tends to decay for points that are separated farther apart in space and time, with the assumption that the correlation between data points is a function only of the time between the samples. Thus, Eq. (23) can be rewritten in terms of the autocorrelation as

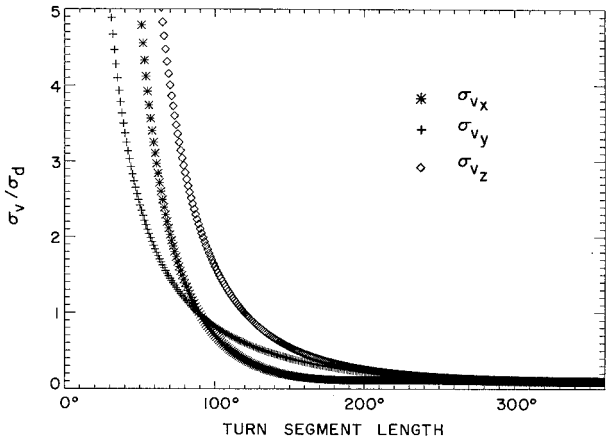

FIG. 4. Standard deviation of the velocity component estimates as a function of the length of the turn segment used. One independent Doppler velocity sample per degree is assumed along with an effective elevation angle of 30° and with the beam initially pointing to the east.

$$\mathrm{var}(\mathbf{V}_i) = \sum_{j=1}^{n} \mathbf{G}_{ij}^{-g}\sigma_d^2 + 2\sum_{j=1}^{n}\sum_{k=j+1}^{n} \mathbf{G}_{ij}^{-g}\mathbf{G}_{ik}^{-g}\sigma_d^2 R(|k-j|), \quad (24)$$

where $R(|k - j|)$ is the autocorrelation between the jth and kth samples. This is not the variance of the component of the wind, but rather the variance of the estimate of that parameter. The standard deviation of the parameter estimates declines rapidly as the length of the turn segment increases. Figure 4 shows the rapid decline in standard deviation of the mean wind terms as a function of the length of the turn segment. This estimate assumes that the variance of the data is constant, that there is one independent sample of velocity per degree, that the radar beam is initially pointed to the east, and that the turn uses a roll angle of 30°. Note from the figure that a 90° turn is a realistic minimum for the AVAD analysis and that significant gains in accuracy can be achieved by using a turn segment closer to 180°. Extending the turn beyond 180° yields only minimal gains in accuracy, while potentially increasing the effects of temporal variations in the wind field. The standard deviation of the parameters for the cases presented was generally between 0.05 and 0.3 m s^{-1}.

The effects of a bias in the Doppler velocities can also be calculated. While a bias is improbable for a ground-based radar, it can easily result from errors in the removal of aircraft motion. The effects of a bias on a given parameter are given by the sum of the weights of the inverse matrix:

$$\mathbf{V}_i = \sum_{j=1}^{n} \mathbf{G}_{ij}^{-g}(\mathrm{V}_{\mathrm{Dopp}_j} + \mathrm{V}_{\mathrm{Bias}}), \quad (25)$$

where $\mathrm{V}_{\mathrm{Bias}}$ is a constant bias included in each velocity measurement. The effects of a bias on different velocity parameters differ depending on the sum of the terms of $\mathbf{G}^{-g}$ for that parameter. The horizontal velocity is unaffected by a bias for turn segments larger than about 20°. A bias has a greater effect on the vertical velocity component and on a higher-order parameter such as divergence. A bias of 1 m s^{-1} corresponding to a 0.6° error in beam pointing direction for an airspeed of 100 m s^{-1} would result in a bias of 1.4 m s^{-1} on the vertical component for a turn with a 45° bank angle and 2 m s^{-2} for a turn with an elevation angle of 30° (side-looking beam with a roll of 30° or up-looking beam with a 60° roll). Errors in the aircraft velocity that are constant for the time of the analysis amount to an inadvertent Galilean transformation and cannot be detected unless the return from the ground or some other reference is included in the analysis. These errors affect all altitudes equally.

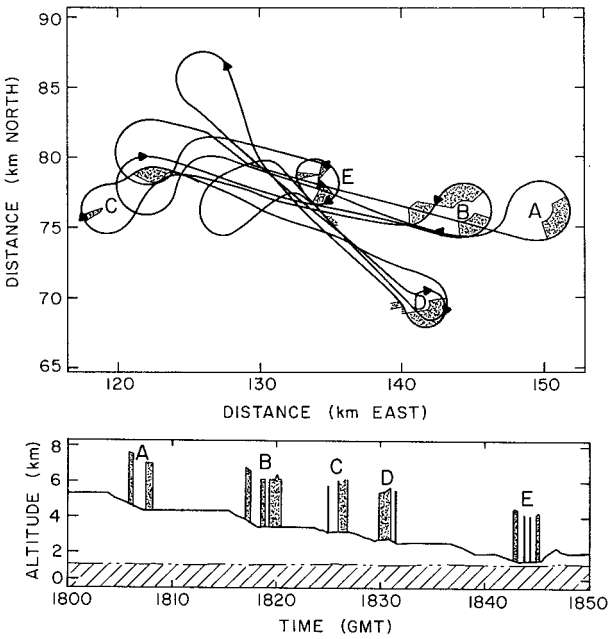

FIG. 5. (a) Map view of flight tracks and areas of coverage for the AVAD analyses. Labels A–E mark the locations of profiles. (b) Flight altitudes and times for the data used in the AVAD analyses. All profiles are up-looking.

4. Results

The AVAD analysis described in the previous sections has been applied to data from two cases: a nimbostratus case from 31 October 1992 and a stratus case from 14 September 1995. These two cases were selected because the wind profiles include several interesting features, there are multiple turn segments with sufficient radar data for the AVAD analysis, and winds measured from the KingAir are available for comparison with the AVAD results.

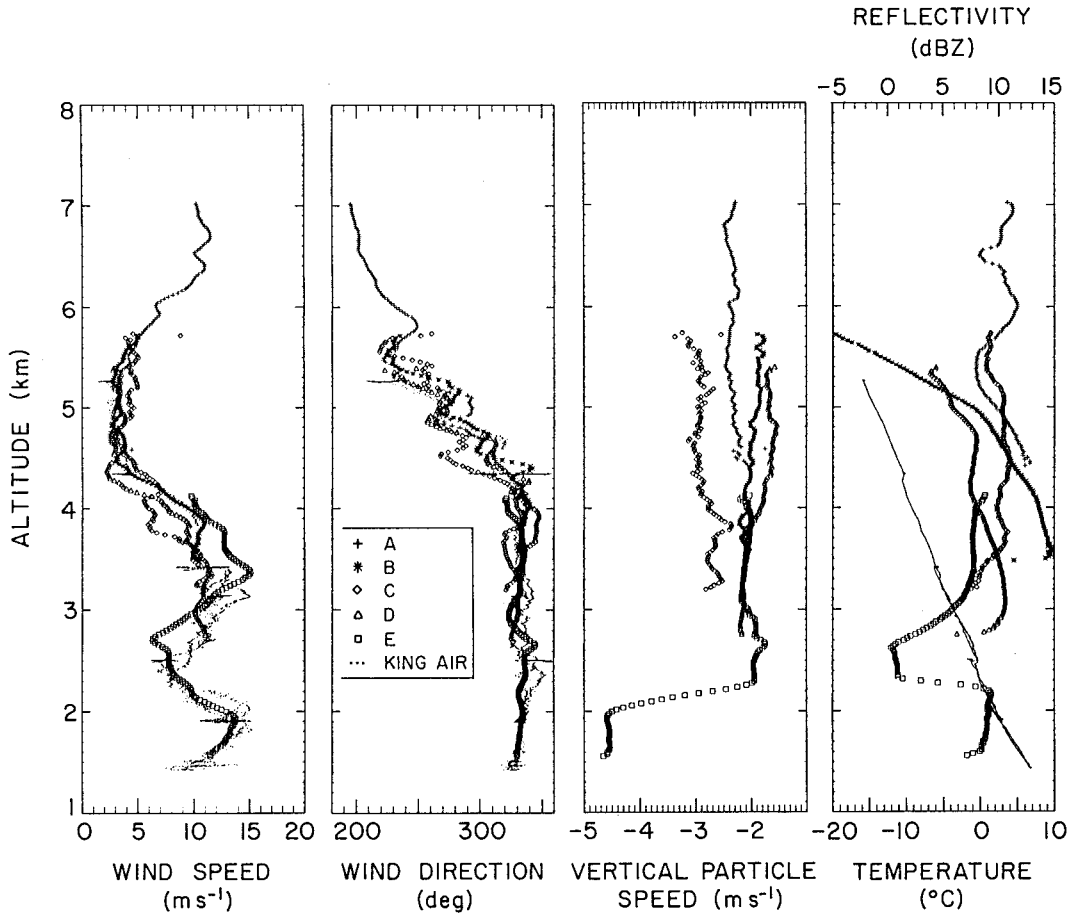

FIG. 6. Wind profiles derived from KingAir data (dots) and AVAD analysis: (a) wind speed, (b) wind direction, (c) vertical particle speed, and (d) temperature and mean reflectivity. Labels A–E on the profiles correspond to the similarly labeled data segments in Fig. 5.

a. Nimbostratus—31 October 1992

The flight on 31 October 1992 was in a nimbostratus that developed to the northeast of Wheatland, Wyoming. The cloud layer extended from below 1.5 km up to almost 9 km (MSL) with precipitation reaching to the ground. Features of interest in this case include a well-defined bright band at the base of a layer of significant shear. Generating cells were embedded near cloud top (8.5 km MSL), and the ice crystals formed in these cells formed high-reflectivity fall streaks that extended through a region of shear and down to a region of uniform reflectivities at 6 km.

The radar beam was fixed in the up-looking position for this flight. The main part of the flight consisted of a series of east–west flight legs conducted at successively decreasing altitudes ranging from 7 to 1.5 km. Data for the AVAD analysis are taken from the turns between flight legs. Radar data files from this day are short, generally less than 1 min of data. Thus, multiple radar data files are incorporated into a single analysis.

This increases the accuracy of the analysis by including a larger range of heading and roll angles. Figure 5 shows the flight track and the data used for the AVAD analyses. Shaded areas mark the radar data used. Five turns have sufficient radar data to attempt the AVAD analysis. The thickness of the cloud layer is over double the radar range of 3 km. A wind profile through the entire depth of the cloud layer must be pieced together from multiple analyses taken at different flight levels. Results from the five AVAD analyses and in situ data from the KingAir are shown in Fig. 6. Between 3 and 5.5 km there are several overlapping profiles, allowing the consistency of the results to be examined, although variations between the profiles may also be due to spatial and temporal variations in the wind field. The most obvious feature in the profile is the melting layer between 2.2 and 2.4 km. In this region fall speeds increase from 1.5 to 4.5 m s^{-1}, while reflectivities increase from 0 to 10 dBZ at the bottom of the melting layer. The wind profiles from the KingAir sounding and the five AVAD analyses show a decrease in wind speeds from 3.3 to 4.5 km. Below 4 km the wind direction remains steady. Above 4 km the winds back sharply at more than 40° km^{-1}. Some minor features are also apparent

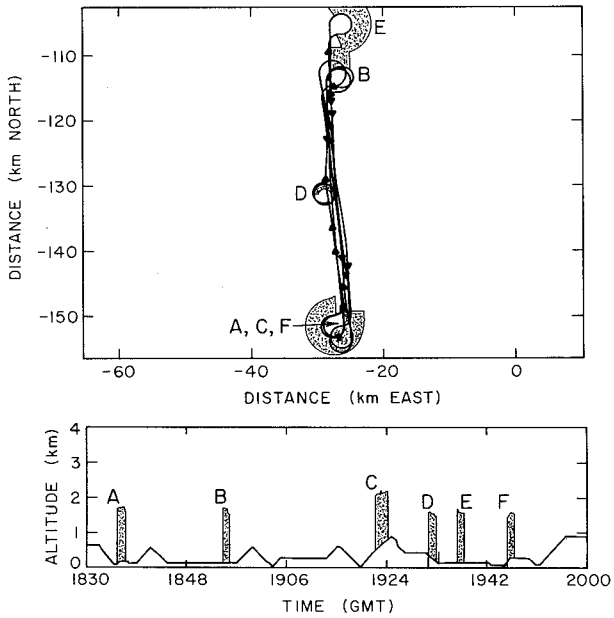

FIG. 7. (a) Map view of flight tracks and areas of coverage for the AVAD analyses. Labels A–F mark the locations of profiles. (b) Flight altitudes and times for the data used in the AVAD analyses. Profiles D and E are side-looking; A, B, C, and F are up-looking.

in several of the profiles. Three or four oscillations in the wind direction of about 30° are evident in the profiles between 4400 and 5500 m, a region in which the wind speeds are steady.

b. Marine stratus—14 September 1995

Observations on this day were made off the coast of Oregon, in a 400-m-thick stratus layer with a distinct cellular structure. Drizzle from the stratus provides sufficient reflectivity to allow the AVAD analysis to be carried out from cloud top all the way to the ocean surface. Average reflectivity increased from −16 to −5 dBZ in the first 100 m below the cloud top and remained nearly constant through the rest of the cloud layer.

The flight consisted primarily of north–south-oriented legs ranging from 25 to 40 km in length. There are seven suitable data segments for the AVAD analysis; however, one of these was too close to cloud top and provided results for only 80 m below cloud top. Of the six profiles used in the composite analysis, four are from the southern end of the flight legs, one is from the northern end, and one is from near the center of the flight legs. These cases are spread over slightly more than 1 h of flight. Figure 7 shows the flight track for this day and the regions used for the AVAD analyses. The composite of the six profiles and the KingAir-measured winds are shown in Fig. 8.

Four of the cases for the radar analysis are from the up-looking setting of the radar beam, while two of the analyses are done with data from the side-looking beam. The up-looking cases provide data from slightly above the flight track (usually about 200 m) to echo top. The side-looking AVAD profiles are taken from 90° to 270° turns and thus give data from both above and below the flight level. In situ winds measured by the KingAir are available from 50 m above the ocean surface to well above cloud top.

Wind speeds increase from roughly 2 m s^{-1} at 200 m and reached 7 m s^{-1} near cloud top. Between 200 and 350 m the mean shear is over 27 m s^{-1} km^{-1}. Below 200 m wind speeds increase to 4 m s^{-1} at the ocean surface. Particle fall speeds remain fairly steady declining from about −1.1 m s^{-1} to −0.9 m s^{-1} near cloud top. Near the 200-m level, winds change from 180° below to 330° above that level. The wind shear evident in the AVAD profiles can also be observed in the reflectivity images. A representative north–south cross section of reflectivity from 14 September is shown in Fig. 9. The wind shear seen between 200 and 400 m in the AVAD profiles is also evident in the cross section, as shown by the curvature of the high-reflectivity fall streaks. The cross section is almost parallel to both the wind and the wind shear vectors. The total shear between 200 and 400 m can be deduced from the final slope of the fall streaks to be between four and six times the fall speed of the scatterers; this is consistent with the AVAD-determined 5–7 m s^{-1} velocity difference between 200 and 400 m for scatterers with a fall speed of between −0.9 and −1.1 m s^{-1}.

Overall, the KingAir-and AVAD-retrieved winds show good agreement with the wind speeds and directions measured by the KingAir. Individual AVAD-derived profiles are very smooth in the vertical. Thus, it seems probable that the spread in the KingAir-measured wind speeds and directions as well as the difference between AVAD profiles is due to real variations in the wind field. There are no consistent spatial or temporal trends in wind speed or direction as most data from the different analyses fall within 2 m s^{-1} and 10° of each other. The vertical particle speeds, in the range of −0.9 to −1.1 m s^{-1} are consistent with those of drizzle drops of radius 0.1–0.2 mm (Beard 1976), which were observed on this day. The side-looking AVAD analyses, D and E, produce poor quality estimates of the vertical particle velocity. The problems with these vertical velocities are primarily due to the low roll angles (<30°) and a small amount of data, which cause the vertical component of motion to be poorly resolved and allow residual aircraft motion to contaminate the vertical component.

5. Conclusions

The AVAD analysis has been shown to be a useful tool for retrieving wind profiles. The data required for the AVAD analysis can generally be obtained from turns required as part of a flight plan. Analyses can be obtained from 45 s of data and 90° of a turn.

The ability to obtain multiple AVAD profiles allows

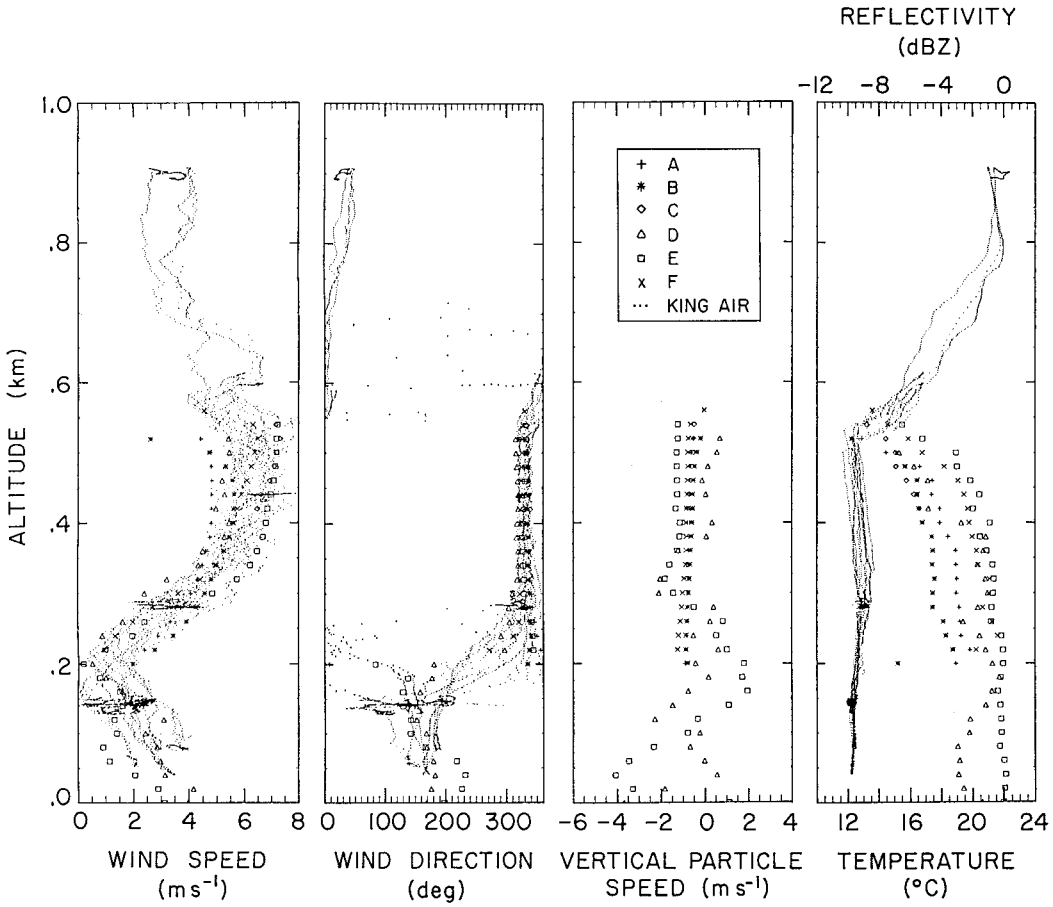

FIG. 8. Wind profiles derived from KingAir data (dots) and AVAD analysis: (a) wind speed, (b) wind direction, (c) vertical particle speed, and (d) temperature and mean reflectivity. Labels A–F on the profiles correspond to the similarly labeled data segments in Fig. 7.

for the identification of small or transient features such as the oscillations in wind direction evident between 4.5 and 6 km in Fig. 6. Whereas time and other constraints may limit the number of aircraft soundings practical to one or two, it is possible to obtain tens of AVAD profiles during a typical 2–3-h research flight.

The AVAD analysis provides data on a scale that begins to bridge the gap between the mesoscale information provided by ground-based VAD analysis or multiple-Doppler techniques and the data provided by the in situ probes. This data helps to provide a context for the in situ data.

This technique is applicable where there are clouds with areas of detectable reflectivity greater than 2 km in diameter. However, the technique is not appropriate in cases where there is significant nonlinear variation of the winds across the analysis region, as is likely in small rapidly growing cumulus.

The variations about the least squares value (as shown in Fig. 3) are perhaps the most interesting area of the AVAD analysis for further exploration. The Doppler velocities from the 14 September case and others show apparently regular oscillations about the least squares fit value. These variations are particularlly evident in Fig. 3, where they appear as semiregular variations of the Doppler velocity about the mean value having a period of about 5 s (or about 400 m at 90 m s^{-1}). These variations may be due to either small-scale velocity structures or to the radar data slicing through higher fall speed fall streaks. The features display a high degree of vertical continuity and can be seen to evolve from one level to the next, thus precluding the possiblitiy that they are artifacts caused by incorrect aircraft motion removal. These features may play a critical role in organizing the cellular structure evident on that day. A nonlinear optimization method similar to that employed by Testud et al. (1980) should be capable of identifying the wavelength and orientation of these waves. Due to the narrow beamwidth and the proximity of the radar to the analysis region it should be possible to identify features with wavelengths less than 100 m.

Acknowledgments. This work has been supported by NSF Grant ATM-9319907 and ONR Grant N0014-93-

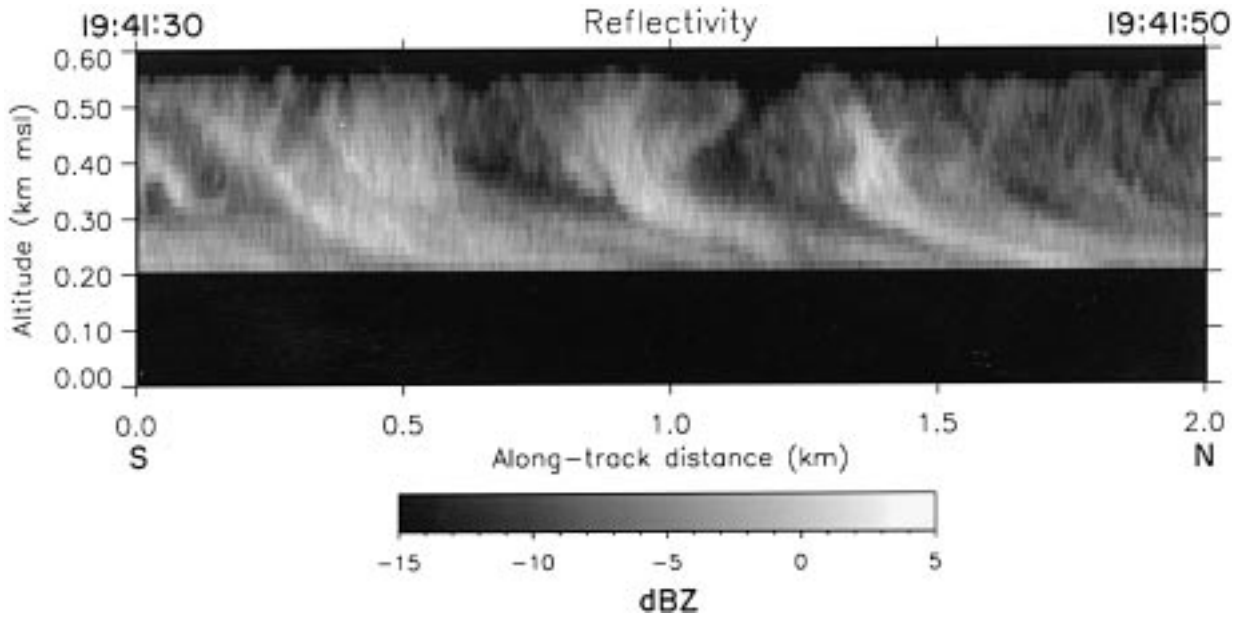

FIG. 9. South–north reflectivity cross section. The curvature of the high-reflectivity fall streaks demonstrates the wind-relative shear present between 200 and 400 m.

1-1248. Susan Allen helped extensively with the preparation of the figures. Jeff Frech contributed greatly to the development of aircraft motion removal software. Discussions with John Galloway provided valuable insight into subtleties of aircraft motion estimation and related timing issues. Thanks also to KingAir facility staff, including the pilots, Ernie Gasaway and George Bershinsky, and to Glenn Gordon for his work processing the KingAir data. Andy Pazmany, Robert McIntosh, and others at the University of Massachusetts,Quadrant Engineering, designed and built the radar used in this analysis.

REFERENCES

Beard, K. V., 1976: Terminal velocity and shape of cloud and precipitation drops aloft. *J. Atmos. Sci.,* **33,** 851–864.

Bevington, P. R., 1969: *Data Reduction and Error Analysis for the Physical Sciences.* McGraw-Hill, 336 pp.

Browning, K. A., and R. Wexler, 1968: The determination of kinematic properties of a wind field using Doppler radar. *J. Appl. Meteor.,* **7,** 105–113.

Easterbrook, C. C., 1975: Estimating horizontal wind fields by two dimensional curve fitting of single Doppler radar measurements. Preprints, *16th Conf. on Radar Meteorology,* Houston, TX, Amer. Meteor. Soc., 214–219.

Jorgensen, D. P., T. Matejka, and J. D. DuGranrut, 1996: Multi-beam techniques for deriving wind fields from airborne Doppler radars. *J. Meteor. Atmos. Phys.,* **59,** 83–104.

Lee, W.-C., P. Dodge, F. D. Marks, and P. H. Hildebrand, 1994: Mapping of airborne Doppler radar data. *J. Atmos. Oceanic Technol.,* **11,** 572–578.

Lenschow, D. H., 1971: The measurement of air velocity and temperature using the NCAR Buffalo aircraft measuring system. NCAR Tech. Note NCAR TN/EDD-74, 39 pp. [Available from National Center for Atmospheric Research, Boulder, CO 80307.]

Lhermitte, R., and D. Atlas, 1961: Precipitation motion by pulse Doppler. Preprints, *Ninth Conf. on Weather Radar,* Kansas City, KS, Amer. Meteor. Soc., 218–223.

Menke, T., 1989: *Geophysical Data Analysis: Discrete Inverse Theory.* Academic Press, 289 pp.

Probert-Jones, J. R., 1960: Meteorological use of pulsed Doppler radar. *Nature,* **186,** 271–273.

Testud, J., G. Breger, P. Amayenc, M. Chong, B. Nutten, and A. Sauvaget, 1980: A Doppler radar observation of a cold front. Three-dimensional air circulation, related precipitation system and associated wave-like motions. *J. Atmos. Sci.,* **37,** 78–98.